Chinese Journal of Electronics
Vol.32, No.6, Nov. 2023

Stability Improvement for One Cycle Controlled Boost Converters Based on Energy Balance Principle

WANG Lei[1], WU Qinghua[2], MA Wei[3], and TANG Wenhu[2]

(1. *Guangzhou Maritime University, Guangzhou 510725, China*)

(2. *South China University of Technology (SCUT), Guangzhou 510641, China*)

(3. *Chongqing University of Science and Technology, Chongqing 401331, China*)

Abstract — Boost converters with one cycle control (OCC) are prone to exhibit oscillations as the Hopf bifurcation, which may degrade performances and limit the parameter stable region of converters. This work proposed a novel control strategy for suppressing such bifurcations and enlarging the parameter stability region of the boost system on the basis of the principle of energy balance in the circuit. Through analyzing of the stability and bifurcation condition, the results reflect that, the energy-based OCC can adjust the poles of the system transfer function, which ensures the stable operation of the system in an extended range of circuit parameters. Moreover, the orders of the transfer function will not be increased by such adjustments, thus the computational complexity of the transfer function will be increased. The theoretical analysis demonstrates the ability of the energy-based OCC for suppressing the bifurcations and enlarging the stable region of the system parameters. The results by simulation and experiment further prove the effectiveness of the proposed control strategy.

Key words — Boost converter, Dynamic average-value model, Bifurcation, Energy balance.

I. Introduction

As a typical control method, one cycle control (OCC) has great developed because of its simple control structure, fast dynamic responses and other advantages [1]–[4]. However, as intrinsic nonlinearity of switching converters, abundant nonlinear phenomena has been introduced within this family of converters, such as Neimark-Sacker bifurcation, secondary bifurcation, even chaos, etc. [5]–[9]. Thus, it is prone to exhibit such nonlinear phenomena in converters using the OCC. An OCC controlled Cuk converter was analyzed using a model based on the sampled data, and Neimark-Sacker bifurcation were observed with some parameters varying [10]. Studies in [11] on a OCC boost converter illustrated that it could work stably in period I state in the discontinuous current mode (DCM), but it could not remain stable in continuous current mode (CCM), and low-frequency oscillations may occur. In [12], low-frequency oscillation was presented in boost converters using a constant-on-time (COT) OCC, and the bifurcation was observed as the COT value increased.

These nonlinear phenomenas cause an adverse impact on the normal running and damages to the converters. Hence, suppressing such nonlinear phenomena is essential. Two types of methods for controlling and suppressing such nonlinear phenomenas have been adopted widely, i.e., feedback and non-feedback methods. For feedback control strategies, the Ott-Grelogi-Yorke (OGY), the occasional proportional feedback (OPF), the time delay feedback (TDF) are typical ones. The adaptive strategy, the resonant parametric is common non-feedback method. Since the OGY is difficultly realized [13], the TDF becomes a useful and common method. But researchers showed that it is always hard to obtain the delayed feedback signals [14], [15]. Thus as an alternative method, a notch or second-order filter was introduced, but there are three parameters which we need to measure, i.e. the feedback gain, the quality factor and the selective frequency [16], [17]. In comparison, only two parameters, the feedback gain and the delayed time, needs to be determined by using the TDF.

Manuscript Received Aug. 31, 2021; Accepted Oct. 1, 2022. This work was supported by the National Natural Science Foundation of China (62001169).

 DOI:10.23919/cje.2021.00.204

A washout filter was implemented to suppress such bifurcation, where the required measurement parameters are reduced to be two. So far, however, no detained calculation methods are introduced. To eliminate such nonlinear phenomena, a TDF controller based on a first-order-filter was proposed. Compared with the conventional second-filter-based TDF, only two parameters must be determined. By contrast, the non-feedback control strategies, which are simpler, appear to be more functional for applying in practice. The resonant parametric strategy is one of typical representative, which was proved that, without extra devices, it can control some nonlinear phenomena in converters effectively [18], [19]. But some parameters must be perturbed within appropriate amplitudes and frequencies, only then can a chaotic be converted to be a regular operation.

Recently, it has been verified that memristive loads can broaden the stable region without affecting bifurcation structures [20]. Compared to conventional capacitor current ripple (CCR) control method, a novel capacitor current and capacitor voltage ripple (CCVR) method has been introduced for a single-inductor dual-output (SIDO) CCM buck converter to extend the load range [21]. The paper presents an energy-based OCC strategy for the conventional OCC converters to suppress the oscillation phenomena and enlarge the stable parameter domains. Compared to the previous studies, there is no parameters need to be defined and no increase in the system order number.

This paper is organized as follows: In Section II, the design and implementation, as well as the stability analysis of the energy-based OCC, are described; The conventional OCC converter is analyzed based on its average model and Hopf bifurcation is found and analyzed in Section III; Section IV gives the results of the simulation and experiment; And Section V summarizes achievements in the work.

II. Stability Analyzing of Boost Converters Based on Energy Balance Principle

The OCC boost converters are prone to exhibit oscillations as the Hopf bifurcation, which may degrade performances of converters. For the purpose of suppressing the bifurcations and stabilising such unstable system, the energy balance principle in the circuit is used for designing the strategy. The implementation and analysis of a boost converter implemented by the energy-based OCC is depicted as below.

1. The design of the energy-based OCC and its implementation

Fig.1 illustrates the diagram of an energy-based OCC boost converter. In Fig.1, $u_{\rm in}$ is the voltage flowing into the converter, i represents the current flowing through L, $i_{\rm o}$ denotes the current flowing through R, $i_{\rm c}$ represents the current across C, $u_{\rm ref}$ denotes the reference voltage and $T_{\rm s}$ denotes the switching cycle.

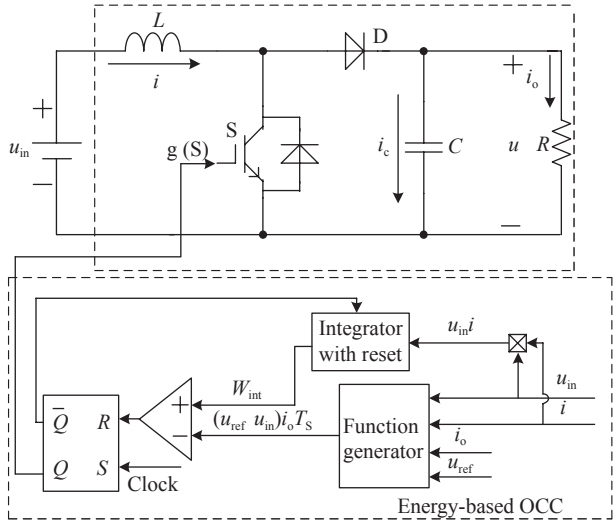

Fig. 1. Block diagram of a boost with the proposed control strategy.

Such a converter in CCM can be described as

$$\begin{aligned}\frac{{\rm d}i}{{\rm d}t} &= \frac{1}{L}u_{\rm in} - \frac{1-s}{L}u,\\ \frac{{\rm d}u}{{\rm d}t} &= -\frac{1}{RC}u + \frac{1-s}{C}i\end{aligned} \tag{1}$$

where $s=0$ means switch S is off, and $s=1$ means S is on.

In addition, the state analysis shows that, during the nth switching period, there are two operating states of the CCM boost converter:

State 1: S is on for duration $t_{\rm on}(n)$, in this operating state, L absorbed energy and the capacitor C offers the energy that the load consumed,

$$W_{L_{\rm in}} = u_{\rm in} i t_{\rm on} \tag{2}$$

$$W_{C_{\rm out}} = u i_{\rm o} t_{\rm on} \tag{3}$$

State 2: S is off for duration $t_{\rm off}(n)$, in this operating state, L releases energy, and the capacitor C is charged,

$$W_{L_{\rm out}} = (u - u_{\rm in}) i t_{\rm off} \tag{4}$$

$$W_{C_{\rm in}} = u(i - i_{\rm o}) t_{\rm off} \tag{5}$$

The principle of the energy-based OCC boost converter is rooted on the energy balance of L and C. What it means is that the inductor and the capacitor absorb and release an equal amount of energy separately in a switching cycle. According to the above analysis, the average model of the energy balance can be

obtained as

$$u_{\text{in}} i t_{\text{on}} = (u - u_{\text{in}})\, i t_{\text{off}} \tag{6}$$

$$u i_{\text{o}} t_{\text{on}} = u(i - i_{\text{o}}) t_{\text{off}} \tag{7}$$

By rearranging equation (7), i can be derived as the following:

$$i t_{\text{off}} = i_{\text{o}} T_{\text{s}} \tag{8}$$

Then substituting (8) into (6), equation (6) is rewritten as

$$u_{\text{in}} i t_{\text{on}} = (u - u_{\text{in}}) i_{\text{o}} T_{\text{s}} \tag{9}$$

Replace u in the right of (9) by u_{ref} since the goal is to make u equal to u_{ref}, and the duty ratio d is obtained as

$$d = \frac{(u_{\text{ref}} - u_{\text{in}}) i_{\text{o}}}{u_{\text{in}} i} \tag{10}$$

According to (10), during the nth switching period, the control equation can be acquired as

$$\int_{(n-1)T_{\text{s}}}^{(n-1)T_{\text{s}} + t_{\text{on}}(n)} u_{\text{in}} i \mathrm{d}t = (u_{\text{ref}} - u_{\text{in}}) i_{\text{o}} T_{\text{s}} \tag{11}$$

Equation (11) is achieved through a reset integrator, a comparator and a RS trigger.

From Fig.1, it can be seen that the integrator starts operation at the start of the nth switching cycle, then S is turned on, at the same time W_{int} increases and is compared instantaneously to the control reference. Once W_{int} reaches the control reference, a pulse for resetting is sent from the comparator, which reset the RS trigger. Then S shutdown and W_{int} is reseted to zero. S remains off until the next clock pulse, then the $(n+1)$th cycle starts.

2. The analysis of the stability

Substituting d in (10) for s in (1), the average model of the proposed energy-based OCC boost converter can be got as following [5]:

$$\begin{aligned} \frac{\mathrm{d}i}{\mathrm{d}t} &= \frac{1}{L} u_{\text{in}} - \frac{1}{L}\left[1 - \frac{(u_{\text{ref}} - u_{\text{in}})u}{u_{\text{in}} i R}\right] u, \\ \frac{\mathrm{d}u}{\mathrm{d}t} &= -\frac{1}{RC} u + \frac{1}{C}\left[1 - \frac{(u_{\text{ref}} - u_{\text{in}})u}{u_{\text{in}} i R}\right] i \end{aligned} \tag{12}$$

Setting the values of $\frac{\mathrm{d}i}{\mathrm{d}t}$ and $\frac{\mathrm{d}u}{\mathrm{d}t}$ of (12) to be 0, then the system equilibrium point is found as

$$\begin{aligned} V &= V_{\text{ref}} \\ I &= \frac{V_{\text{ref}}^2}{V_{\text{in}} R} \\ D &= \frac{V_{\text{ref}} - V_{\text{in}}}{V_{\text{ref}}} \end{aligned} \tag{13}$$

where V_{ref} is the value of the output reference, and V_{in} is the value of the input voltage.

Neglecting the input voltage perturbation, the small-signal model of the CCM boost converter around this equilibrium point is expressed as

$$\begin{aligned} \frac{\mathrm{d}\hat{i}}{\mathrm{d}t} &= \frac{V}{L}\hat{d} - \frac{1-D}{L}\hat{u} \\ \frac{\mathrm{d}\hat{u}}{\mathrm{d}t} &= -\frac{1}{RC}\hat{u} + \frac{1-D}{C}\hat{i} - \frac{I}{C}\hat{d} \end{aligned} \tag{14}$$

where $\hat{i}$, $\hat{u}$, $\hat{d}$ represent the small-signal perturbations of i, u and d, respectively.

Transform (14) into the frequency domain and eliminate $\hat{i}$, the linearized small-signal transfer function is derived:

$$\frac{\hat{u}(s)}{\hat{d}(s)} = K_{\text{v}} \frac{-\frac{s}{Q_{\text{v}}\omega_0} + 1}{\frac{s^2}{\omega_0^2} + \frac{s}{Q_{\text{v}}\omega_0} + 1} = K_{\text{v}} \frac{D_{\text{vd}}(s)}{N_{\text{vd}}(s)} \tag{15}$$

where $K_{\text{v}} = \frac{V}{1-D}$, $Q_{\text{v}} = (1-D)R\sqrt{\frac{C}{L}}$, $\omega_0 = \frac{1-D}{\sqrt{LC}}$, $D_{\text{vd}}(s) = -\frac{s}{Q_{\text{v}}\omega_0} + 1$ and $N_{\text{vd}}(s) = \frac{s^2}{\omega_0^2} + \frac{s}{Q_{\text{v}}\omega_0} + 1$.

Based on (10), at this system equilibrium point, the linearized small-signal model is given as follows:

$$\hat{d} = \frac{1}{V}\hat{u}_{\text{ref}} + \frac{D}{V}\hat{u} - \frac{D}{I}\hat{i} \tag{16}$$

According to [22], [23], the sample and hold effect $H_{\text{e}}(s)$ should be considered, which is simplified as

$$H_{\text{e}}(s) = 1 + \frac{s}{Q_{\text{z}}\omega_{\text{n}}} + \frac{s^2}{\omega_{\text{n}}^2} \tag{17}$$

where $\omega_{\text{n}} = \frac{\pi}{T_{\text{s}}}$, $Q_{\text{z}} = -\frac{2}{\pi}$.

Transform (16) into the frequency domain by eliminating $\hat{i}$ and considering $H_{\text{e}}(s)$:

$$\hat{d}(s) = H_{\text{e}}(s)\frac{1}{K_{\text{v}}}\frac{s\hat{u}_{\text{ref}}(s) + B(s)\hat{u}(s)}{A(s)} \tag{18}$$

where $A(s) = (1-D)s + DQ_{\text{v}}\omega_0$, $B(s) = D + DQ_{\text{v}}\omega_0$.

Substitute (15) into (18), the linearized small-signal function of the energy-based OCC is formed as below:

$$\frac{\hat{u}(s)}{\hat{u}_{\text{ref}}(s)} = \frac{sH_{\text{e}}(s)D_{\text{vd}}(s)}{A(s)N_{\text{vd}}(s) - B(s)H_{\text{e}}(s)D_{\text{vd}}(s)} \tag{19}$$

After obtaining the transfer function of the energy-based OCC boost converter, the following part gives the derivation of the sufficient conditions, under which the system is stable by studying the properties of roots for the corresponding characteristic equation.

First, setting the value of the denominator in (19) to zero, then the characteristic equation in the equilibri-

um point of (13) is found as

$$A(s)N_{\rm vd}(s) - B(s)H_{\rm e}(s)D_{\rm vd}(s) = 0 \tag{20}$$

Then third-order Pade approximation is used to get a closed-form expression to analyze the converter stability. By using the third-order Pade approximation, equation (20) can be written as follows:

$$\begin{aligned} &N(s) = a_3 s^3 + a_2 s^2 + a_1 s + a_0 \\ &a_3 = \frac{D}{Q_{\rm v}\omega_0\omega_{\rm n}^2} \\ &a_2 = \frac{1-D}{\omega_0^2} + \frac{D}{Q_{\rm v}\omega_0 Q_{\rm z}\omega_{\rm n}} \\ &a_1 = \frac{1}{Q_{\rm v}\omega_0} + \frac{DQ_{\rm v}}{\omega_0} - \frac{DQ_{\rm v}\omega_0}{\omega_{\rm n}^2} \\ &a_0 = 1 - \frac{DQ_{\rm v}\omega_0}{Q_{\rm z}\omega_{\rm n}} \end{aligned} \tag{21}$$

The Routh array of this third-order system is shown as Table 1. According to the Routh stability criterion, all the roots are on the left-half plane, which is condition for stability. And that a_i are all positive and the coefficients in the first column are all positive are the sufficient and prerequisite conditions to ensure that the roots are all on the left-half plane. And the number of the roots with positive real part and times the element symbols in the first column changes are equal. Observing the Routh array of this third-order system shown in Table 1, it is clear that $a_3 > 0$ and $a_0 > 0$. According to the Routh criterion, the condition ensuring the stability of the energy-base OCC are listed as

$$\begin{cases} a_1 > 0 \\ a_2 > 0 \\ A_1 = \dfrac{a_2 a_1 - a_3 a_0}{a_2} > 0 \end{cases} \tag{22}$$

Table 1. The Routh array of third-order system

s^3	a_3	a_1
s^2	a_2	a_0
s^1	A_1	0
s^0	a_0	0

Note: $A_1 = \frac{a_2 a_1 - a_3 a_0}{a_2}$.

By solving (22), the condition ensuring stability by the duty ratio is calculated as the following:

$$D_{\rm c} = \frac{2RC}{T_{\rm s} + 2RC} \tag{23}$$

Subsequently, the analysis results of the system is summarized in the following:

Case 1: $D < D_{\rm c}$, the converter system operates stably, which works at the damped oscillation mode.

Case 2: $D > D_{\rm c}$, the converter system loses stable, which working at the increased oscillation mode. As a result, Hopf bifurcation occurs, as D crosses the stable boundary $D_{\rm c}$.

The analysis demonstrates that $D_{\rm c}$ depends on circuit parameters listed in Table 2. Based on such parameters, $D_{\rm c}$ of the energy-based OCC boost converter can be calculated to be 0.993 according to (23), which is close to 1. It is observed that the stable parameter domains of the boost system using the energy-based OCC is enlarged. Thus there is no Hopf bifurcation and other nonlinear phenomenons in almost the entire parameter region.

Table 2. The circuit parameters

$u_{\rm in}$ (V)	L (μH)	C (μF)	R (Ω)	$f_{\rm s}$ (Hz)
5	3000	460	30	5000

III. Stability Analyzing of Boost Converters with OCC

In fact, the conventional OCC is on the basis of volt-second balance principle of the inductor L, which is

$$d = \frac{t_{\rm on}}{T_{\rm s}} = \frac{u_{\rm ref} - u_{\rm in}}{u} \tag{24}$$

Substituting d for s in (1), the average model of the conventional OCC is calculated as

$$\begin{aligned} \frac{{\rm d}i}{{\rm d}t} &= \frac{1}{L}u_{\rm in} - \frac{1}{L}\left(1 - \frac{u_{\rm ref} - u_{\rm in}}{u}\right)u, \\ \frac{{\rm d}u}{{\rm d}t} &= -\frac{1}{RC}u + \frac{1}{C}\left(1 - \frac{u_{\rm ref} - u_{\rm in}}{u}\right)i \end{aligned} \tag{25}$$

Let the values of $\frac{{\rm d}i}{{\rm d}t}$ and $\frac{{\rm d}u}{{\rm d}t}$ in (25) equal to be 0, then the system equilibrium point is calculated:

$$\begin{aligned} V &= V_{\rm ref} \\ I &= \frac{V_{\rm ref}^2}{V_{\rm in}R} \\ D &= \frac{V_{\rm ref} - V_{\rm in}}{V_{\rm ref}} \end{aligned} \tag{26}$$

Using (24), the linearized small-signal model is derived as

$$\hat{d} = \frac{1}{V}\hat{u}_{\rm ref} - \frac{D}{V}\hat{u} \tag{27}$$

Transform (27) into the frequency domain, the linearized small-signal model can be derived as

$$\hat{d}(s) = H_{\rm e}(s)\frac{\hat{u}_{\rm ref}(s) - D\hat{u}(s)}{V} \tag{28}$$

Substitute (15) into (28), the linearized small-signal function of the OCC boost is obtained:

$$\frac{\hat{u}(s)}{\hat{u}_{\mathrm{ref}}(s)}=\frac{H_{\mathrm{e}}(s)D_{\mathrm{vd}}(s)}{(1-D)N_{\mathrm{vd}}(s)+DH_{\mathrm{e}}(s)D_{\mathrm{vd}}(s)} \tag{29}$$

Setting the value of the denominator in (29) as zero, the characteristic equation in the equilibrium point of (26) is obtained as

$$(1-D)N_{\mathrm{vd}}(s)+DH_{\mathrm{e}}(s)D_{\mathrm{vd}}(s)=0 \tag{30}$$

By using such a third-order Pade approximation, (30) is written as follows:

$$\begin{aligned}
&N(s)=a_3s^3+a_2s^2+a_1s+a_0\\
&a_3=-\frac{D}{Q_{\mathrm{v}}\omega_0\omega_{\mathrm{n}}^2}\\
&a_2=\frac{(1-D)}{\omega_0^2}+\frac{D}{\omega_{\mathrm{n}}^2}-\frac{D}{Q_{\mathrm{v}}\omega_0Q_{\mathrm{z}}\omega_{\mathrm{n}}}\\
&a_1=\frac{1-2D}{Q_{\mathrm{v}}\omega_0}+\frac{D}{Q_{\mathrm{z}}\omega_{\mathrm{n}}}\\
&a_0=1
\end{aligned} \tag{31}$$

Observing the Routh array of this third-order system shown in Table 1, it is clear that $a_3<0$ and $a_0>0$. Since $a_3<0$, even if $a_1>0$, $a_2>0$ and $A_1>0$ are satisfied, the symbols change once in the first column, so the polynomial equation $N(s)=0$ has one root with positive real parts. Thus, the system is not stable. However, since this pole is the non-dominant pole, the dynamic performance of the system is mainly determined by the other two poles. Thus, if $a_1>0$, $a_2>0$ and $A_1>0$ are satisfied, these two poles are conjugate complex poles with negative real parts. Then the conditions should be met for stability requirements as follows:

$$\begin{cases}
a_1>0\\
a_2>0\\
A_1=\dfrac{a_2a_1-a_3a_0}{a_2}>0
\end{cases} \tag{32}$$

By solving (32), the condition to ensure the stability for the duty ratio is

$$D_{\mathrm{c}}=\sqrt[3]{-\frac{q}{2}+\sqrt{\Delta}}+\sqrt[3]{-\frac{q}{2}-\sqrt{\Delta}}+\frac{2}{3} \tag{33}$$

where $\Delta=\left(\frac{q}{2}\right)^2+\left(\frac{p}{3}\right)^3$, $p=-\frac{1}{3}+\frac{4L}{RT_{\mathrm{s}}}$ and $q=\frac{2}{27}+\frac{2L}{3RT_{\mathrm{s}}}$.

With the parameters in Table 2, D_{c} of the OCC boost converter can be calculated to be 0.43 according to (33). Thus, for the conventional OCC, when $D>0.43$ is met with the variation of the system parameters, for example, u_{ref}, R, L, etc., the system is unstable and the Hopf bifurcation occurs.

Compared with D_{c} of the energy-based OCC boost converter calculated by (23), it is observed that the stable parameter domains of the boost system using the energy-based OCC are enlarged. The Hopf bifurcation and other nonlinear phenomenons are suppressed and the system can operate stably in most of the entire parameter region.

IV. Simulation and Experiment

In this section, a simulation model and an experimental CCM boost converter are built respectively. In the study, u_{ref} is selected as the variable parameter. To highlight the function of the proposed energy-based OCC for suppressing the Hopf bifurcation and enlarging the stable domains of the parameters, the proposed energy-based OCC is in contrast to that of the conventional OCC.

Based on such parameters, the threshold reference voltage u_{refc} of the conventional OCC boost converter can be calculated to be $u_{\mathrm{refc}}=\frac{u_{\mathrm{in}}}{1-D_{\mathrm{c}}}=8.774$ V according to (33). Table 3 provides the domain poles of the energy-based OCC boost converter under varied u_{ref}. The poles are obtained from (14). In Table 3, when $u_{\mathrm{ref}}=8$ V, the real parts of the system domain poles are negative, the real parts of the domain poles are always negative with the value increasing of u_{ref}. Even as u_{ref} increases to 20 V, the real parts of the domain poles are still negative. Such results mean that the roots always locate on the left-half plane, which means the converter work stably even though u_{ref} varies widely. Bifurcation diagram is shown in Fig.2. From Fig.2, it is found that, even when u_{ref} increases to be 15 V, the energy-based OCC boost converter remains stable operation.

Table 3. The domain poles of the energy-based OCC boost converter under varied u_{ref}

u_{ref}	Poles (p_1 and p_2)	State
8 V	$p_1=-2235,\ p_2=-233.4$	Stable
9 V	$p_1=-2424,\ p_2=-190.1$	Stable
10 V	$p_1=-2500,\ p_2=-164.4$	Stable
11 V	$p_1=-2516,\ p_2=-147.1$	Stable
⋮	⋮	⋮
15 V	$p_1=-2367,\ p_2=-111.4$	Stable
⋮	⋮	⋮
20 V	$p_1=-2125,\ p_2=-91.39$	Stable

Table 4 lists the domain poles of the conventional OCC boost converter by varying u_{ref}, which are obtained from (30). From Table 4, it can be observed that, when $u_{\mathrm{ref}}\leq 8.7$ V, the real component of the system domain poles is negative. This illustrates that these roots are located on the left-half plane. Apparently, the converter keeps stable. However, with the increasing of u_{ref}, the roots move towards the right-half plane gradu-

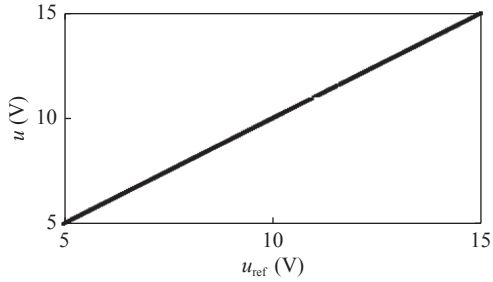

Fig. 2. Bifurcation figures of the energy-based OCC boost with variation of u_{ref}.

ally. As shown in Table 4, when $u_{ref} \geq 8.8$ V, which is greater than u_{refc}, the real part of the domain poles turns into positive, meaning that the roots are located in the right-half plane. Then the Hopf bifurcation happens and the system losses its stability. From Fig.3, such results are observed from its bifurcation diagram, which shows that, when u_{ref} is grater than about 8.774 V, the Hopf bifurcation happens in the OCC boost converter.

Table 4. The domain poles of the conventional OCC boost converter under varied u_{ref}

u_{ref}	Poles (p_1 and p_2)	State
8 V	$-6.010 \pm$ j671.3	Stable
8.5 V	$-2.125 \pm$ j651.0	Stable
8.7 V	$-0.606 \pm$ j643.4	Stable
8.8 V	$0.147 \pm$ j639.7	Unstable
10 V	$8.934 \pm$ j599.5	Unstable
⋮	⋮	⋮
15 V	$43.56 \pm$ j485.9	Unstable
⋮	⋮	⋮
20 V	$77.46 \pm$ j413.8	Unstable

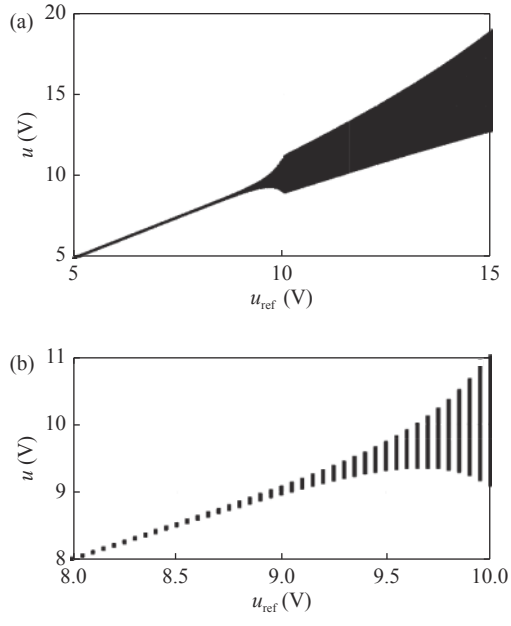

Fig. 3. Bifurcation figures of the conventional OCC boost with variation of u_{ref}. (a) Original drawing; (b) Partial enlarged drawing.

Figs.4 and 5 are the u-i phase portrait of the boost with the energy-based and conventional OCC. From the results, it can be found, when $u_{ref} = 8$ V even increasing to 20 V, the energy-based boost converter remains stable throughout. In contrast, Fig.5 illustrates that, using the conventional OCC, the converter can operate stably under $u_{ref} = 8$ V. However, when $u_{ref} = 10$ V, the phase orbital diagram becomes the torus, at the moment, the converter operates in the state of Hopf bifurcation. And with the increasing of u_{ref}, the phase portrait illustrates that other nonlinear phenomena occurs.

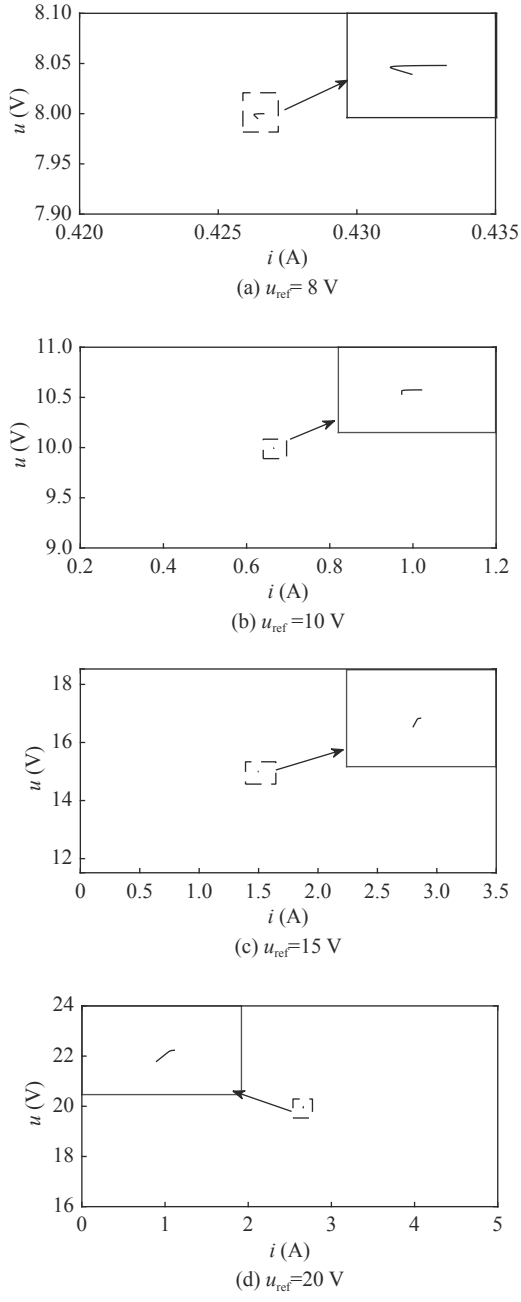

Fig. 4. The u-i phase portrait of the energy-based OCC boost converter.

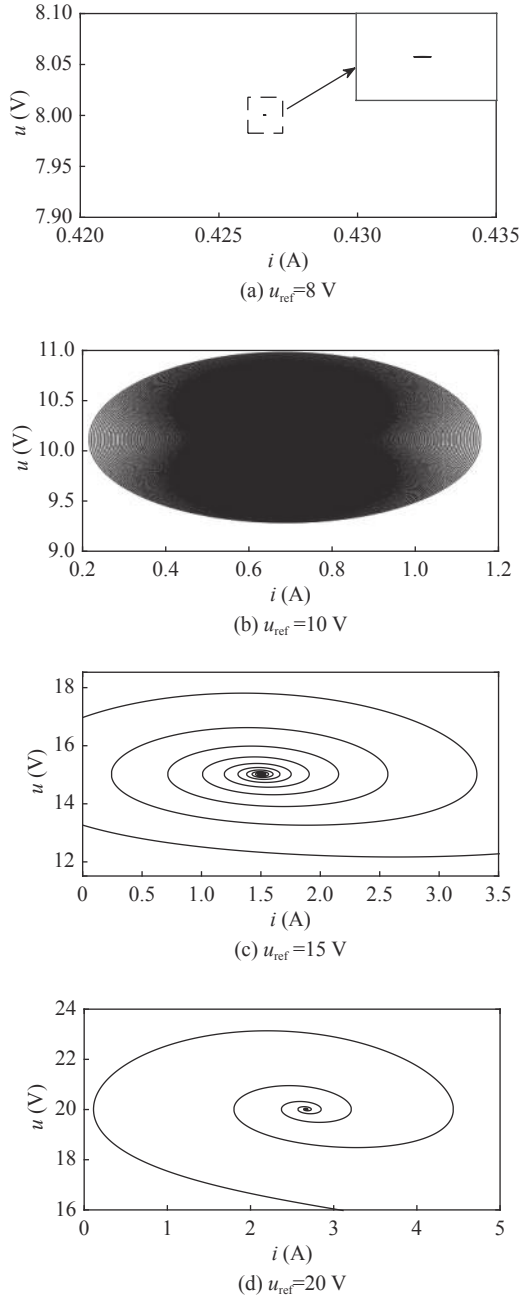

Fig. 5. The u-i phase portrait of the conventional OCC boost converter.

1. Simulation results

Figs.6–9 display the results of the energy-based OCC boost. The results show that, under $u_{\text{ref}} = 8$ V and $u_{\text{ref}} = 10$ V, the system operates stable without bifurcations or other nonlinear phenomena. However, when u_{ref} increases to 15 V and even 20 V, the system remain stable operations.

In contrast, Figs.10–13 display the simulation results with the conventional OCC. In Fig.10, it is observed that, under $u_{\text{ref}} = 8$ V, without bifurcations or other nonlinear phenomena, thus, the system works stably. Fig.11 shows the results of the converter under

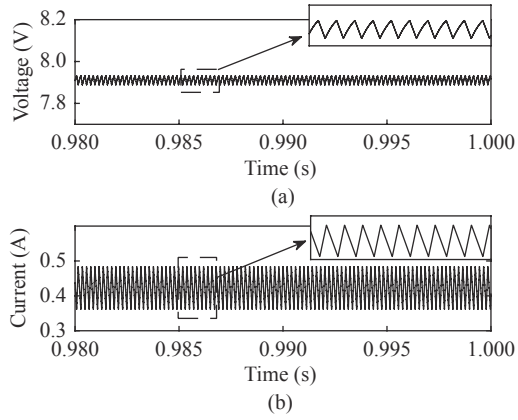

Fig. 6. Simulation results when $u_{\text{ref}} = 8$ V using the energy-based OCC. (a) u; (b) i.

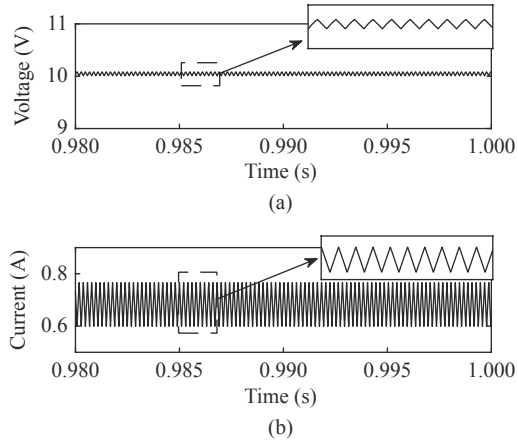

Fig. 7. Simulation results when $u_{\text{ref}} = 10$ V using the energy-based OCC. (a) u; (b) i.

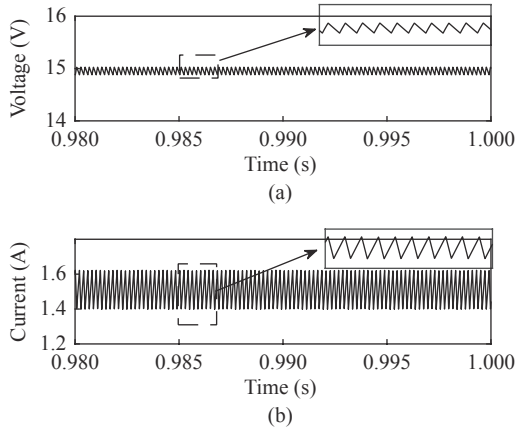

Fig. 8. Simulation results when $u_{\text{ref}} = 15$ V using the energy-based OCC. (a) u; (b) i.

$u_{\text{ref}} = 10$ V. From Fig.8, it is observed that i exhibits Hopf bifurcation, leading to output voltage oscillations. Clearly, the converter is no longer stable. When u_{ref} continues to increase, the bifurcation still exists and the oscillation is more severe, even causing the discontinuous operation of the inductor current, as shown in Figs.12 and 13.

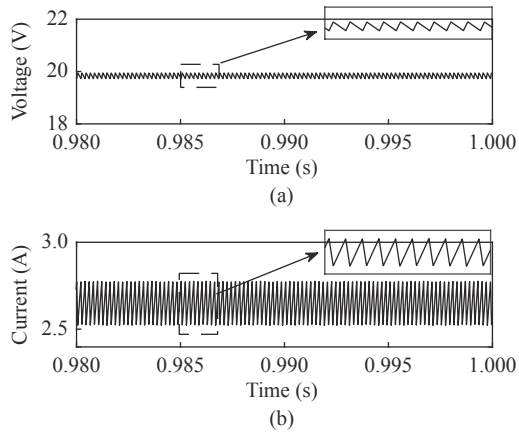

Fig. 9. Simulation results when $u_{\text{ref}} = 20$ V using the energy-based OCC. (a) u; (b) i.

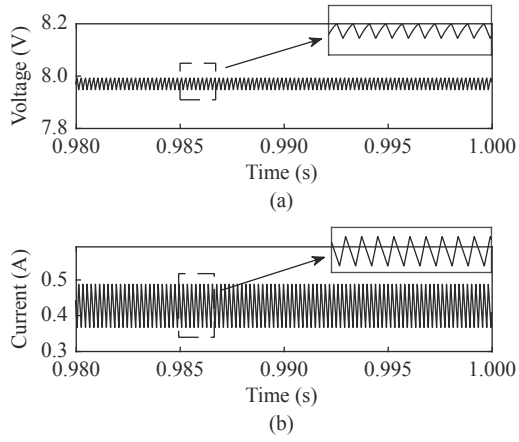

Fig. 10. Simulation results of the conventional OCC when $u_{\text{ref}} = 8$ V. (a) u; (b) i.

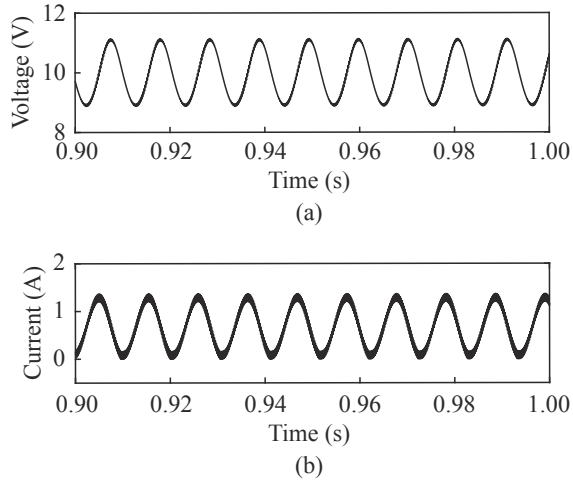

Fig. 11. Simulation results of the conventional OCC when $u_{\text{ref}} = 10$ V. (a) u; (b) i.

2. Experimental results

For further verifying the performances of the energy-based OCC method. The experimental prototypes are built according to the parameters in Table 2. In experiments, SKM75GAL063D and Skyper32R board 1 are used to build the circuit. And the StarSim is used to implement the control part. The sample circuit is achieved by HALL sensors, where the HALL sensors are used to measure the value of the current and voltage. The voltage conversion ratio between the value of the measured voltage u_{m} and that of the practical value u_{p} is as follows:

$$\frac{u_{\text{p}}}{u_{\text{m}}} = 10 \tag{34}$$

The current conversion ratio between the value i_{m}

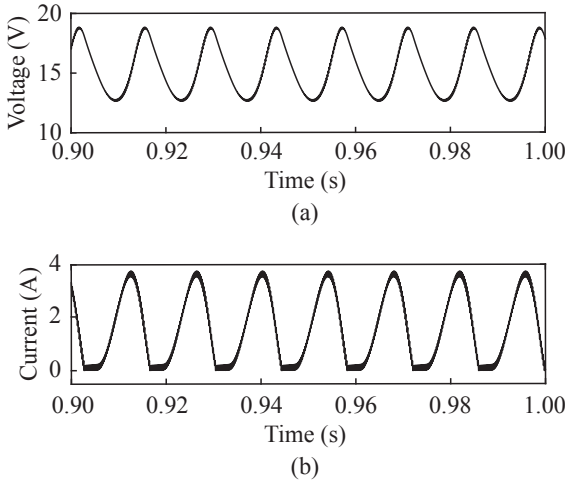

Fig. 12. Simulation results of the conventional OCC when $u_{\text{ref}} = 15$ V. (a) u; (b) i.

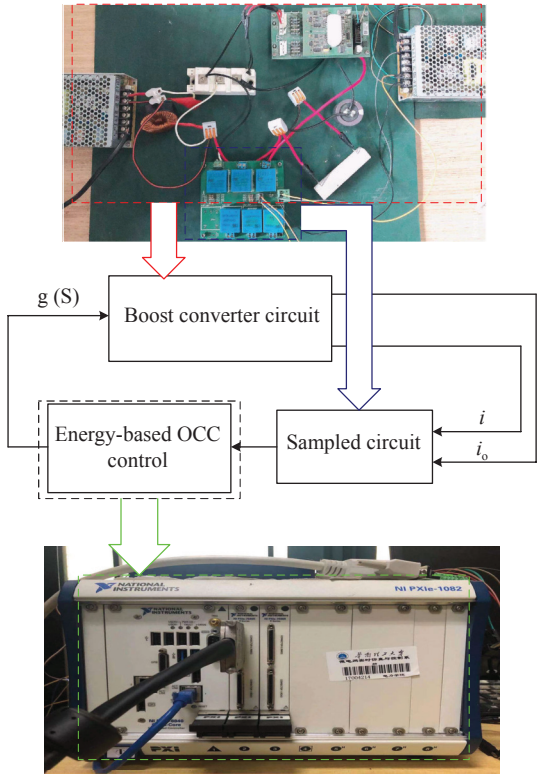

Fig. 13. Experimental prototype.

and the practical value i_{p} is as follows:

$$\frac{i_{\mathrm{p}}}{i_{\mathrm{m}}} = \frac{i_{\mathrm{p}} R_{\mathrm{m}}}{u_{\mathrm{mc}}} = 1.16 \tag{35}$$

where R_{m} represents the resistor for sensing, the value of which is 116 Ω, and u_{mc} represents the voltage value produced by the flowing of i_{m} through R_{m}.

Figs.14 and 15 provide the results from experiment by varying u_{ref}. In Fig.14, it is observed that, with the energy-based OCC, the converter can operate in the stable state under $u_{\mathrm{ref}} = 8$ V. With the increasing of u_{ref}, the converter is always operate stably. Even u_{ref} is increased to 20 V, it can still keep stable operation. In contrast, using the conventional OCC, under $u_{\mathrm{ref}} = 8$ V, the system maintains stable operation without any nonlinear behavior. But when u_{ref} is increased to be 10 V, as greatly as u_{refc}, the converter loses stable and Hopf bifurcation occurs in the inductor

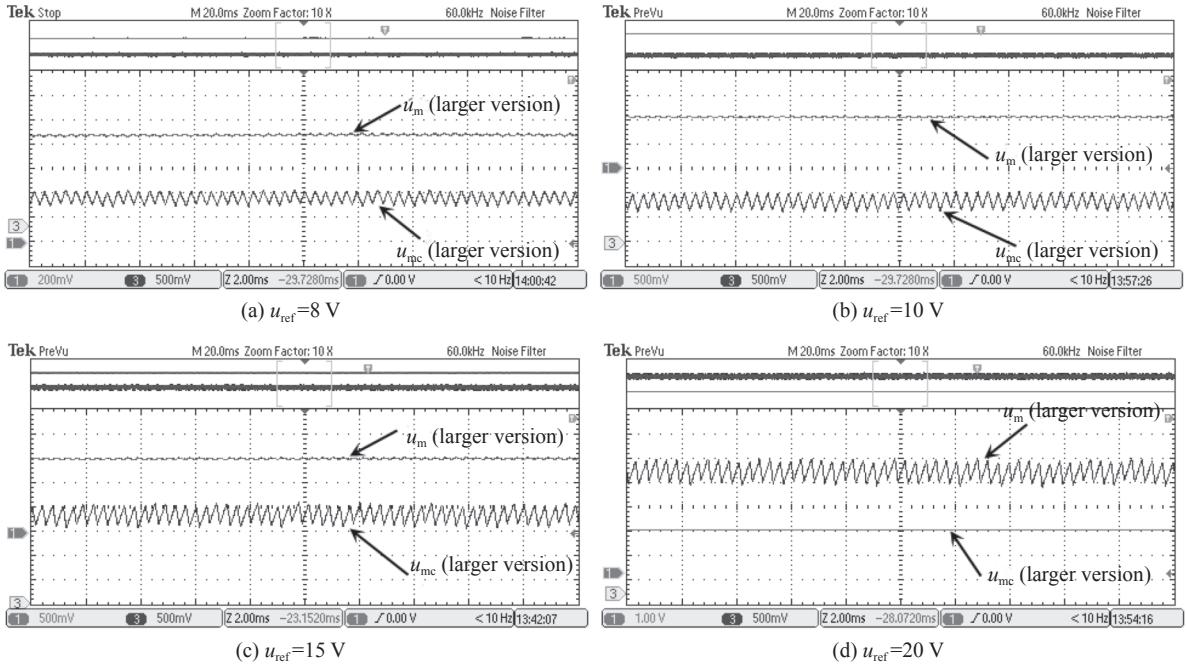

(a) u_{ref}=8 V (b) u_{ref}=10 V

(c) u_{ref}=15 V (d) u_{ref}=20 V

Fig. 14. Results by experiment of the proposed strategy.

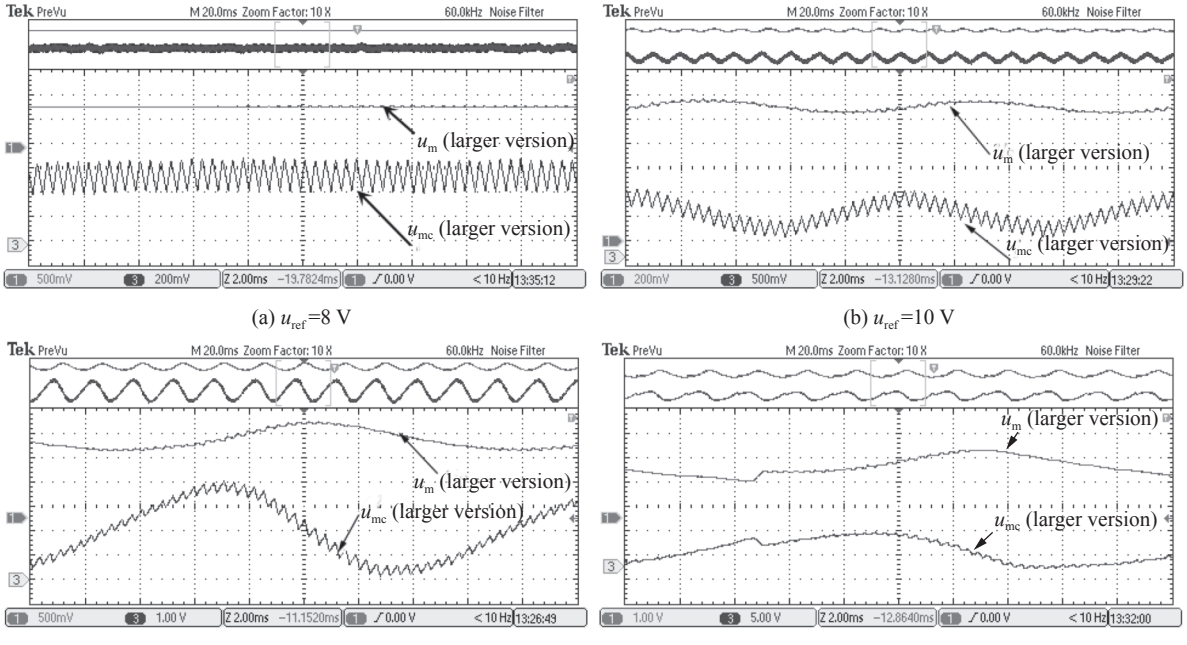

(a) u_{ref}=8 V (b) u_{ref}=10 V

(c) u_{ref}=15 V (d) u_{ref}=20 V

Fig. 15. Results by experiment of the conventional OCC.

current. With the continuous increasing of $u_{\rm ref}$, the bifurcation still exists and the oscillation is more severe, just as Fig.15. The analysis illustrates that the experimental results are coincident with that of the theoretical analysis and simulation, which demonstrate that, in contrast to that of the OCC, the energy-based OCC can suppress the oscillation and enlarge the system stable parameter domains.

V. Conclusions

In the paper, for the purpose of enlarging the parameter stable region of the system, an energy-based OCC method is proposed. In the view of control principle, in this study, the volt-second balance principle on which the conventional OCC is based is replaced by the energy balance of the circuit. The theoretical analysis results demonstrate that the bifurcation can be suppressed and the stable parameter domains of the system is extended. Take the reference output voltage as an example, results from simulation and experiment validate the theoretical analysis. It illustrates, in contrast to that of the conventional OCC, the proposed strategy can suppress the bifurcations and possesses an extended stable parameter domain. Besides, the system this work discussed is based on boost, and the proposed strategy can be applied to buck, buck-boost and other types of converters.

References

[1] Z. R. Lai, K. M. Smedley, and Y. H. Ma, "Time quantity one-cycle control for power-factor correctors," *IEEE Transactions on Power Electronics*, vol.12, no.2, pp.369–375, 1997.

[2] C. M. Qiao, T. T. Jin, and K. M. Smedley, "One-cycle control of three-phase active power filter with vector operation," *IEEE Transactions on Industrial Electronics*, vol.51, no.2, pp.455–463, 2004.

[3] A. A. De Melo Bento and E. R. C. Da Silva, "Hybrid one-cycle controller for boost PFC rectifier," *IEEE Transactions on Industry Applications*, vol.45, no.1, pp.268–277, 2009.

[4] K. Subramanian, V. K. S. Kumar, E. M. Saravanan, *et al.*, "Improved one cycle control of dc-dc buck converter," in *Proceedings of IEEE International Conference on Advanced Communications, Control and Computing Technologies*, Ramanathapuram, India, pp.219–223, 2014.

[5] A. El Aroudi, D. Giaouris, H. H. C. Iu, *et al.*, "A review on stability analysis methods for switching mode power converters," *IEEE Journal on Emerging and Selected Topics in Circuits and Systems*, vol.5, no.3, pp.302–315, 2015.

[6] W. Hu, B. Zhang, and R. Yang, "Bifurcation mechanism and stabilization of V^2C controlled buck converter," *IEEE Access*, vol.7, pp.77174–77182, 2019.

[7] A. E. Aroudi, R. Haroun, M. Al-Numay, *et al.*, "Fast-scale stability analysis of a DC-DC boost converter with a constant power load," *IEEE Journal of Emerging and Selected Topics in Power Electronics*, vol.9, no.1, pp.549–558, 2021.

[8] H. M. Wu, V. Pickert, M. Y. Ma, *et al.*, "Stability study and nonlinear analysis of DC-DC power converters with constant power loads at the fast timescale," *IEEE Journal of Emerging and Selected Topics in Power Electronics*, vol.8, no.4, pp.3225–3236, 2020.

[9] X. Zhang, Z. W. Zhang, H. Bao, *et al.*, "Stability effect of control weight on multiloop COT-controlled buck converter with PI compensator and small output capacitor ESR," *IEEE Journal of Emerging and Selected Topics in Power Electronics*, vol.9, no.4, pp.4658–4667, 2021.

[10] Y. L. Guo, L. Wang, and Q. H. Wu, "Control of Neimark-Sacker bifurcation in one cycle controlled Cuk converters," in *2020 IEEE 29th International Symposium on Industrial Electronics (ISIE)*, Delft, Netherlands, pp.95–99, 2020.

[11] J. P. Wang, L. K. Hou, L. Zhang, *et al.*, "Analysis of the low-frequency oscillation phenomenon in constant-on-time controlled boost converter," in *2015 IEEE Energy Conversion Congress and Exposition (ECCE)*, Montreal, QC, Canada, pp.1571–1574, 2015.

[12] W. Hu, B. Zhang, R. Yang, *et al.*, "Dynamic behaviours of constant on-time one-cycle controlled boost converter," *IET Power Electronics*, vol.11, no.1, pp.160–167, 2018.

[13] K. Pyragas, "Continuous control of chaos by self-controlling feedback," *Physics Letter A*, vol.170, no.6, pp.421–428, 1992.

[14] A. E. Aroudi, R. Haroun, A. Cid-Pastor, *et al.*, "Suppression of line frequency instabilities in PFC AC-DC power supplies by feedback notch filtering the pre-regulator output voltage," *IEEE Transactions on Circuits and Systems I:Regular Papers*, vol.60, no.3, pp.796–809, 2013.

[15] W. G. Lu, P. Y. Xu, L. W. Zhou, *et al.*, "Bifurcation control of current-mode buck converter via TDFC," *Chinese Physics Letters*, vol.27, no.3, article no.0305011, 2010.

[16] W. G. Lu, L. W. Zhou, Q. M. Luo, *et al.*, "Filter based non-invasive control of chaos in buck converter," *Physics Letters A*, vol.372, no.18, pp.3217–3222, 2008.

[17] C. H. Cai, Z. Y. Xu, W. B. Xu, *et al.*, "Notch filter feedback control in a class of chaotic systems," *Automatica*, vol.38, no.4, pp.695–701, 2002.

[18] T. Banerjee, D. Biswas, and B. C. Sarkar, "Design and analysis of a first order time-delayed chaotic system," *Nonlinear Dynamics*, vol.70, no.1, pp.721–734, 2012.

[19] A. Kavitha and G. Uma, "Control of chaos by resonant parametric perturbation in a current mode controlled buck-boost Dc-Dc converter," in *2008 Twenty-Third Annual IEEE Applied Power Electronics Conference and Exposition*, Austin, TX, USA, pp.323–327, 2008.

[20] B. C. Bao, X. Zhang, H. Bao, *et al.*, "Dynamical effects of memristive load on peak current mode buck-boost switching converter," *Chaos, Solitons & Fractals*, vol.122, pp.69–79, 2019.

[21] Y. Wang, J. P. Xu, F. B. Qin, *et al.*, "A capacitor current and capacitor voltage ripple controlled SIDO CCM buck converter with wide load range and reduced cross regulation," *IEEE Transactions on Industrial Electronics*, vol.69, no.1, pp.270–281, 2022.

[22] W. Tang, F. C. Lee, R. B. Ridley, *et al.*, "Charge control: Modeling, analysis, and design," *IEEE Transactions on Power Electronics*, vol.8, no.4, pp.396–403, 1993.

[23] R. B. Ridley, "A new, continuous-time model for current-mode control (power convertors)," *IEEE Transactions on Power Electronics*, vol.6, no.2, pp.271–280, 1991.

WANG Lei received the B.E. and M.S. degrees in electrical engineering from Chongqing University, China, in 2008 and 2011, respectively, and Ph.D. degree in electrical engineering from the South China University of Technology, Guangzhou, China, in 2016. She is currently an Associate Professor with Guangzhou Maritime University. Her research interests include renewable energy integration in power grids, modeling and control of power converters, and nonlinear analysis of power electronics. (Email: w.lei19@mail.scut.edu.cn)

WU Qinghua received the Ph.D. degree in electrical engineering from The Queen's University of Belfast (QUB), Belfast, UK in 1987. He worked as a Research Fellow and subsequently a Senior Research Fellow in QUB from 1987 to 1991. He joined the Department of Mathematical Sciences, Loughborough University, Loughborough, UK in 1991, as a Lecturer, subsequently he was appointed Senior Lecturer. In September 1995, he joined The University of Liverpool, Liverpool, UK to take up his appointment to the Chair of Electrical Engineering in the Department of Electrical Engineering and Electronics. Currently, he is with the School of Electric Power Engineering, South China University of Technology, Guangzhou, China, as a Distinguished Professor and the Director of Energy Research Institute of the University. Professor Wu has authored and coauthored more than 440 technical publications, including 220 journal papers, 20 book chapters and 3 research monographs published by Springer. He is a Fellow of IEEE, Fellow of IET, Chartered Engineer and Fellow of InstMC. His research interests include nonlinear adaptive control, mathematical morphology, evolutionary computation, power quality and power system control and operation. (Email: wuqh@scut.edu.cn)

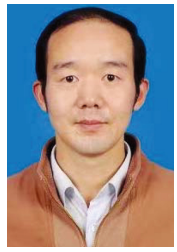

MA Wei received the Ph.D. degree in electrical engineering from Chongqing University, China. He is currently with the Chongqing University of Science and Technology, where he teaches courses on electrical engineering. His research interests include power converter modeling, nonlinear phenomena, and the application of power converters. (Email: cqustma@cqust.edu.cn)

TANG Wenhu (corresponding author) received the B.E. and M.S. degrees in electrical engineering from the Huazhong University of Science and Technology, Wuhan, China, in 1996 and 2000, respectively, and the Ph.D. degree in electrical engineering from The University of Liverpool, Liverpool, UK, in 2004. He was a Postdoctoral Research Associate and subsequently a Lecturer at The University of Liverpool between 2004 and 2013. He is currently a Distinguished Professor and the Dean of the School of Electric Power Engineering, South China University of Technology, Guangzhou, China. He has authored and coauthored more than 100 research papers, including 40 journal papers and 1 Springer research monograph. His research interests include renewable energy integration in power grids, condition monitoring and fault diagnosis for power apparatus, multiple criteria evaluation, and intelligent decision support systems. (Email: wenhutang@scut.edu.cn)